

Article

A Multipath Process-Based Inherent Strain Method for Prediction of Deformation of Hull Plate for Integrated Heating and Mechanical Rolling Forming Process

Zhenshuai Wei ¹ , Yao Zhao ^{1,2,3,*}, Hua Yuan ^{1,2,3} and Lichun Chang ¹

¹ School of Naval Architecture and Ocean Engineering, Huazhong University of Science and Technology, Wuhan 430074, China

² Collaborative Innovation Center for Advanced Ship and Deep-Sea Exploration (CISSE), Shanghai 200240, China

³ Hubei Key Laboratory of Naval Architecture and Ocean Engineering Hydrodynamics (HUST), Wuhan 430074, China

* Correspondence: yzhaozzz@hust.edu.cn; Tel.: +86-027-8754-3258

Abstract: Integrated heating and mechanical rolling forming (IHMRF) has recently been introduced for manufacturing complex curvature hull plates. It fabricates the target curved plate by sequential loading along the multipath. Accurate and efficient prediction of the deformation of the plate is the basis for developing the process planning and ensuring the quality of the forming. The inherent-strain method is ideal for this purpose, but its prediction accuracy needs to be improved. This paper proposes a multipath process-based inherent-strain method (MPISM), which considers the effect of the sequential loading process of the multipath on plate deformation. First, the effect of loading paths near the plate edge was investigated, which in turn clarified the rationale for obtaining the inherent strain only in the plate center. Secondly, a strain correction strategy was established by analyzing the variation pattern of the inherent strain caused by the crossing or proximity of the previous path and the subsequent path. This allowed the effects of the loading process to be taken into account in the elastic analysis. Based on the plate-and-shell theory, the idea of an equivalent inherent strain distribution is also presented. This makes the loading of inherent strains more accurate in the elastic finite-element model. MPISM predictions and experimental results show good agreement. Compared with the thermo-elastic-plastic finite element method, the MPISM substantially improves efficiency while maintaining accuracy. Compared with the original inherent-strain method, the MPISM is more accurate in terms of deformation magnitude prediction.

Keywords: induction heating; mechanical rolling; inherent strain; hull plate forming; numerical prediction



Citation: Wei, Z.; Zhao, Y.; Yuan, H.; Chang, L. A Multipath Process-Based Inherent Strain Method for Prediction of Deformation of Hull Plate for Integrated Heating and Mechanical Rolling Forming Process. *J. Mar. Sci. Eng.* **2024**, *12*, 654. <https://doi.org/10.3390/jmse12040654>

Academic Editor: José António Correia

Received: 19 March 2024

Revised: 9 April 2024

Accepted: 12 April 2024

Published: 15 April 2024



Copyright: © 2024 by the authors. Licensee MDPI, Basel, Switzerland. This article is an open access article distributed under the terms and conditions of the Creative Commons Attribution (CC BY) license (<https://creativecommons.org/licenses/by/4.0/>).

1. Introduction

Forming steel plates with complex curvature is a critical step in the ship fabrication process. According to the plate-and-shell theory, the plate undergoes shape change due to in-plane and out-of-plane strain generated within the plate. Therefore, forming is the process of inputting the combinations of in-plane and out-of-plane strain into the plate [1]. To satisfy the strain combination requirements of forming, thermal and mechanical processing are frequently alternated in engineering practice [2]. However, switching machining platforms is counterproductive to automation as it adds to the overall complexity of the forming process. The integrated heating and mechanical rolling forming (IHMRF) process was recently introduced for efficiently manufacturing complex curvature hull plates [3]. It combines the advantages of heating and mechanical roll forming by integrating thermal and mechanical loads in one work platform. Integrating thermal and mechanical loads avoids platform switching and facilitates the development of automated systems.

In addition, coupling thermal and mechanical loads enriches the available in-plane and out-of-plane strain combinations.

In IHMRF, the plate is simultaneously subjected to the mechanical bending force of the rollers and the heating action of the heat source, also known as thermo-mechanical loads. When the thermo-mechanical loads applied to the plate cause the stresses in the plate to reach the yield point, plastic deformation will occur at the loading location and its immediate vicinity. Localized plastic deformation will extend along the loading path due to the movement of thermo-mechanical loads along the loading path. The target shape is achieved by controlling the local deformation. This mode of forming is usually referred to as line loading. In order to form the target shape, the process planning needs to be developed first, including determining the magnitude of the thermo-mechanical loads and the arrangement of the loading paths. However, IHMRF is a non-die process, and the relationship between the loading and deformation is complex. As a result, numerous iterative simulations are typically required to identify the ideal planning, which invariably requires a significant number of plate deformation predictions. Therefore, accurate and efficient deformation prediction of deformation in hull plate manufactured through the IHMRF process is essential for developing the process planning and ensuring the quality of the components.

The advantage of the thermo-elastic-plastic finite element method is that it can accurately simulate both the transient and final states of the mechanical behavior by considering all the variables that affect the deformation during the line-loading process [4]. Because of its great accuracy, the method can validate other simplified methods or analyze the mechanisms of the forming process [5]. However, because of the nonlinearities in the TEP-FE analysis of the IHMRF process, such as load movement and temperature-dependent material properties, simulating a single-line-loading process with this method takes a long time. Furthermore, the deformation prediction time for the TEP-FEM becomes even more redundant because numerous loading paths are typically included in the IHMRF process. Despite simplifying the loading model of the TEP-FEM, the computational time consumption remains too high [5]. Therefore, for process planning, the TEP-FEM is not a suitable method for predicting plate deformation. For the process planning of the IHMRF process, a more efficient deformation prediction method must be developed while maintaining computational accuracy.

In contrast, the inherent strain method (ISM) is a simplified method that aims to improve the efficiency of deformation prediction. It obtains the deformation of the workpiece through an elastic analysis with the inherent strain as the load [6]. The inherent strain method was originally proposed to predict the residual deformation of the workpiece during metal welding. In welding, the distribution of residual plastic strain in the workpiece tends to be approximately constant in the middle region of the loading path and is geometrically insensitive [7]. Residual plastic strain represents the inherent effect of the machining process and is often referred to as inherent strain. Experiments or TEP-FE simulations on relatively tiny specimens can be used to derive the inherent strain because its distribution tends to be constant [8]. The computing efficiency is significantly increased by mapping the inherent strain under the same process conditions onto large-scale structures for elastic deformation field analysis. Recently, researchers have found that the distribution of residual plastic strain in machined parts also tends to be constant during line-loading processes including local line rolling, additive manufacturing, and line heating [9–12]. As a result, the ISM has advanced further and is now being applied to predicting deformation in more complex line-loading processes. Nevertheless, research on the use of the ISM for the IHMRF process is lacking.

As mentioned above, the application of the ISM is based on the fact that inherent strain distributions tend to be constant. Therefore, it is necessary, first, to analyze the characteristics of the inherent strain distribution of the IHMRF process. Another problem is that the arrangement of the loading paths for the IHMRF process is more complex than welding. On the one hand, the arrangement of the loading paths is possible at certain

positions on the plate, for example, close to the edge of the plate. The inherent strains may differ due to the constraints of the surrounding material at different locations on the plate. Results may be inconsistent if the inherent strain at one place is applied to other areas. Nonetheless, it will undoubtedly take a long time to determine the inherent strain depending on the position of each loading path. Therefore, it is necessary to discuss the effect of the proximity of the loading path to the edge of the plate on the inherent strain and, thus, to determine a reasonable method for obtaining the inherent strain.

On the other hand, loading paths may cross or be close to each other. The previous and subsequent paths may interact because of residual stress. Existing ISMs do not adequately consider the effects of residual stresses during sequential loading. Therefore, there is a need to clarify these effects and then consider them in the ISM to improve accuracy.

This paper proposes a multipath process-based inherent strain method (MPISM) for efficiently predicting plate deformation by the IHMRF process. It is difficult to measure and observe the inherent strain using experimental methods because of the high-temperature and mechanical-loading conditions of the IHMRF process. As a result, the primary tool used in this study was the experimentally verified TEP-FEM. The distribution characteristics of the inherent strains of the IHMRF process were analyzed, thus clarifying the feasibility of developing an efficient prediction method based on the basic concepts of the ISM. The effects of the proximity of the processing paths to the plate edges and the crossing or proximity between the processing paths on the inherent strain were analyzed, thus giving a method for taking these effects into account.

2. IHMRF Process

Figure 1 shows a schematic diagram of the essential components of the IHMRF process. The process integrates a set of concave–convex rollers and the heat source as a loading tool. Induction heating was chosen as the heat source in this study. The rollers provide both the forming force to bend the plate and the driving force to move the plate in the specified direction. In other words, the loading tool does not move while the plate moves. The rollers and the heat source can rotate simultaneously around the vertical axis, thus enabling the processing in different directions. The inductive heat source is located at fixed distances in front of and behind the rollers and follows the rollers, i.e., its loading path coincides with the rollers. Depending on the needs of the process, a water-cooling device can be used to cool the plates. It can be seen that the IHMRF process is used to form complex curved plates by applying local out-of-plane bending and in-plane shrinkage deformation to the plate.

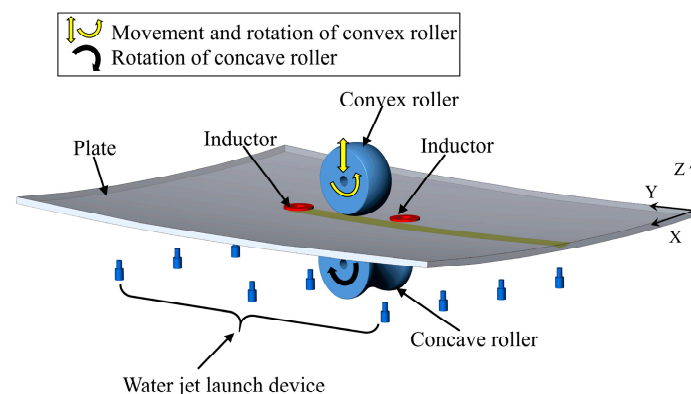


Figure 1. Schematic illustration of the IHMRF process.

3. TEP-FE Analysis of the IHMRF Process

Before the MPISM is presented, the IHMRF process is first simulated by the TEP-FEM. The general characteristics of the inherent strain distribution of the plate in the IHMRF process were clarified based on the TEP-FEM results. In addition, the effects of the proximity

of the loading paths to the plate edges and the intersection or proximity of the loading paths to each other on the inherent strain during the IHMRF process were analyzed.

3.1. TEP-FEM and Experimental Validation

The TEP-FE analysis of the IHMRF process was performed based on ABAQUS software. Due to the negligible influence of mechanical processes on thermal effects in IHMRF, a decoupled thermo-mechanical analysis scheme was adopted. However, the contribution of the transient temperature field to the stresses through thermal expansion was considered. The solution procedure consisted of two steps. Firstly, the temperature history of induction heating was obtained by heat transfer analysis. Thermal radiation and convective heat transfer boundary conditions were considered in the heat transfer analysis. The surface heat source model was used to simulate the induced heat source. Then, the temperature history and mechanical action of the rollers were applied to analyze the mechanical response of the plate. In the mechanical analysis, the mechanical action of the rollers is modeled through equivalent displacement loads. To prevent rigid displacements, a spring constraint is used.

The same mesh with a size of 10 mm × 10 mm was used in heat transfer and mechanical analyses. The ABAQUS element S4R was used for mechanical analyses, and the element DS4 was used for heat transfer analyses. The Mises yield criterion was used to characterize the yielding behavior of the material. The temperature-dependent thermo-physical and mechanical properties were considered in the decoupled analysis.

The experimental validation of the TEP-FEM guarantees the dependability of the outcomes. Figure 2 shows a photograph of the experimental setup. It mainly consists of a control system, a three-axis gantry robot, a heating-rolling unit, a water-jet launch device, and a 3D scanner measurement unit. The geometry and dimensions of the rollers and the induction heat source are shown in Figure 3 and Table 1. Since the main focus of this study was on the ISM, only a brief description of the TEP-FEM validation procedure is provided here, and more information is available in reference [5].

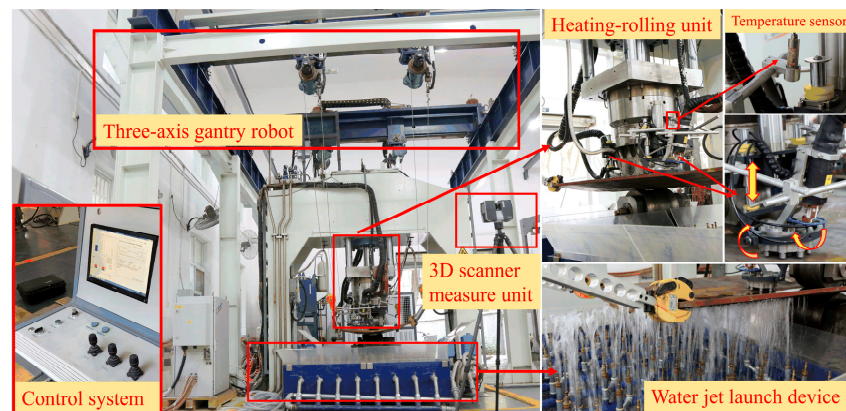


Figure 2. Photograph of the IHMRF experimental setup.

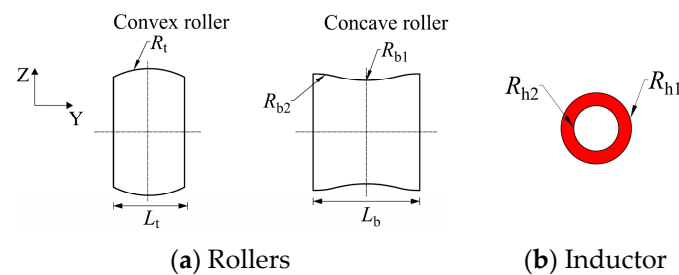


Figure 3. Schematic diagram of shape of the rollers and inductor for IHMRF.

Table 1. Geometry of rollers and inductor.

R_t (mm)	L_t (mm)	R_{b1} (mm)	R_{b2} (mm)	L_b (mm)	R_{h1} (mm)	R_{h2} (mm)
550	200	550	550	300	100	30

3.2. General Characteristics of the Inherent Strain Distribution

As shown in Figure 4, the loading path was the center line in the length direction of the plate. The material of the plate is mild steel Q235, and its geometric dimensions are 1600 mm × 1000 mm × 16 mm. The TEP-FE analysis utilized values for plate thickness h ranging from 15 to 35 mm, forming depth d between 2 and 6 mm, heat source power P between 20 and 40 kW, and plate movement velocity v between 2 and 6 mm/s. Directions parallel to the loading path are classified as longitudinal, and directions perpendicular to the path are transverse.

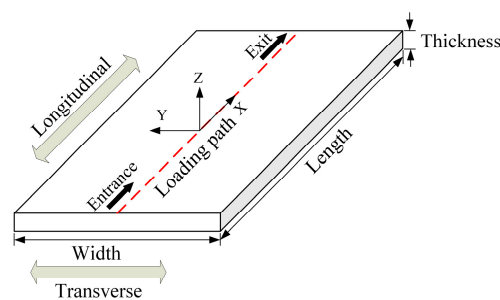
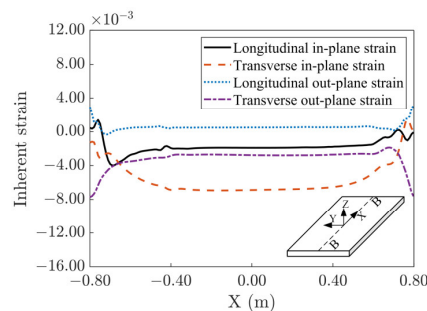
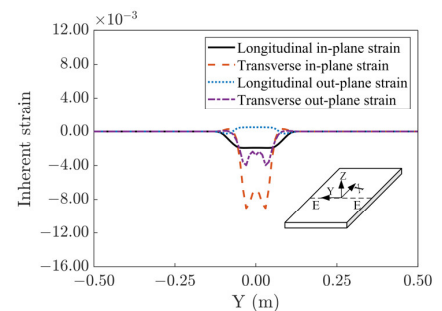


Figure 4. Schematic diagram of the plate model.

Figure 5 illustrates the inherent strain distribution curve of the plate during the IHMRF process. As shown in Figure 5a, the inherent strain varied significantly only near the beginning and end of the loading path, while it remained essentially constant in the middle region. This is because the loads and constraints acting on the material in the middle parts of the loading path were almost identical, resulting in highly similar strains in these areas. However, there were significant temperature and constraint variations near the beginning and end of the loaded loading path and the inherent strain changed correspondingly. As shown in Figure 5b, the values of the inherent strains were relatively complex along the transverse direction, but their larger values were concentrated in the geometrical scale range of the heat source. It should be emphasized that Figure 5 shows the general characteristics of the inherent strain distribution. The inherent strains generated by different process parameters are similar to those in Figure 5, except that the magnitude of the strains may vary. According to the distribution characteristics of inherent strains, it is feasible to develop an efficient prediction method for plate deformation during the IHMRF process based on the basic concepts of the ISM.



(a) Distribution of inherent strain along the longitudinal direction



(b) Distribution of inherent strain along the transverse direction

Figure 5. Distribution of inherent strain.

3.3. The Effect of Loading Paths near the Plate Edge

It is typical to arrange the loading path at various distances from the plate edge during forming. IHMRF loading occurs locally, with deformation centered around the loading path. Consequently, the material away from the loading route acts as a constraint on the line-loading-induced deformation. The strength of the constraint depends on the loading position. Because of symmetry, constraints are the same on both sides of the loading path when it is in the center of the plate. However, the constraints on the side that favors the plate edge may lessen as the loading path approaches one of the plate edges. This means the inherent strain will vary when loading at different positions.

TEP-FE analyses were performed to examine the effect of the loading path near the plate edge on the inherent strain. A line parallel to the plate edge was chosen as the loading line, as seen in Figure 6, and its distances from the plate edge, S , were set at 150 mm, 250 mm, 350 mm, and 500 mm, in that order. The minimal value of S was determined to be 150 mm based on the typical width of rollers used in the IHMRF process. The plate dimensions and loading characteristics remained unchanged from Section 3.2.

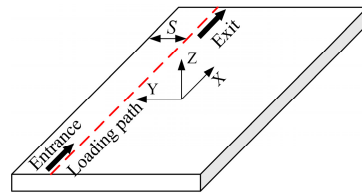


Figure 6. Schematic diagram of the distance from the loading path to the edge of the plate.

The strain distributions under various loading parameters were very similar. The results under one set of loading parameters are analyzed in detail here as an example. The distribution of inherent strains that resulted from varying S values is displayed in Figure 7. The transverse out-of-plane strain, longitudinal out-of-plane strain, longitudinal out-of-plane strain, and longitudinal in-plane strain produced at various distance conditions were all similar. On the other hand, the transverse in-plane strain remained constant for the remaining distance conditions and only reduced at $S = 150$ mm. These findings demonstrate that the distance between the loading path and the plate edge had a negligible impact on the inherent strain within a concise range.

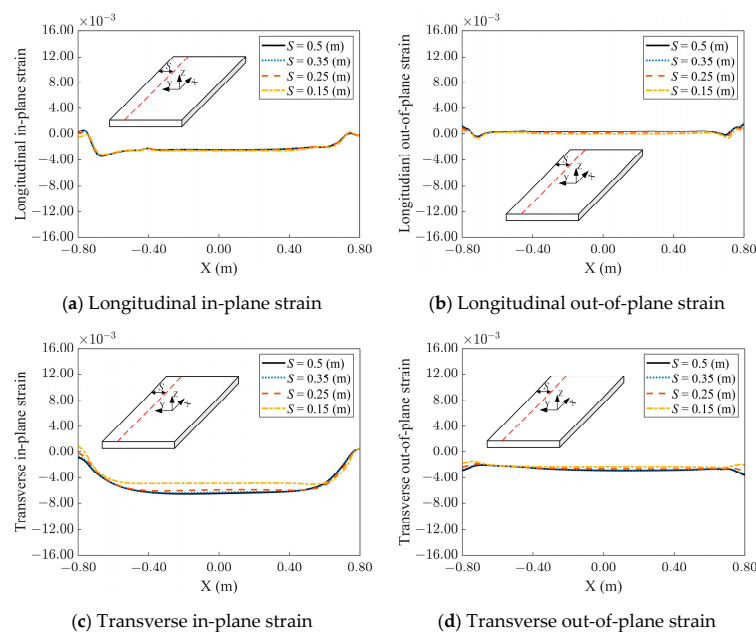


Figure 7. Effect of the distance from the loading path to the plate edge on the inherent strain.

3.4. Effect of Multiple Loading Paths

(1) Effects of loading path crossing

TEP-FE analyses were performed to examine the effect of loading path crossing on the inherent strain. As illustrated in Figure 8, the two loading lines were set to be perpendicular to each other. After completing Path 1 and letting the plate cool to room temperature, Path 2 was carried out. The material characteristics, plate dimensions, and loading parameters were maintained as in Section 3.2.

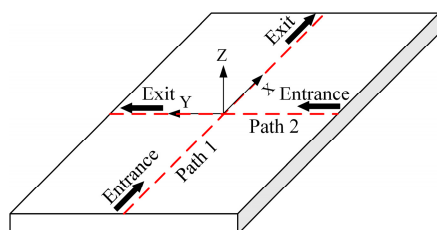


Figure 8. Schematic diagram of cross-loading lines.

The strain distributions under various loading parameters were very similar. The results under one set of loading parameters are analyzed in detail here as an example. The inherent strain distribution along Path 2, as determined by the single-line-loading linear superposition and the cross-loading line TEP-FE analysis, is depicted in Figure 9. The strain distribution of the cross-loaded line in the middle of Path 2 (in Figure 8) differed significantly from the linear superposition of the single-line loading, which happened to be the intersection of the loading line. This indicates that the effect of the cross-loaded line on the strain distribution was primarily concentrated in the vicinity of the intersection point, with the difference between the two paths being smaller in the area beyond the intersection point. Similar results were obtained for Path 1. The difference between the single-line loading linear superposition and the cross-processing approach is primarily associated with the residual stress distribution [13]. In the middle region, Path 1 completion resulted in a substantial x -direction tensile residual stress, whereas the y -direction residual stress was modest. Because the residual stresses were mostly concentrated in this region, the scale range of the strain-affected region was nearly equal to the diameter of the induction heating source used in the analyzed example. As seen in Figure 9b–d, the magnitude of the remaining strain components was more akin to that of a single-loaded linear superposition.

(2) Effect of loading path spacing

In order to analyze the effect of loading path spacing, TEP-FE analyses with two loading paths parallel to each other, as shown in Figure 10, were carried out. In general, as the distance between the two loading paths increased, the overlap area of the plastic zone md, and the interaction between the two loading paths decreased accordingly. In the analyzed example, the values of the loading path spacing W were chosen to be 50 mm and 150 mm, which was selected considering the diameter of a typical induction heating source. The loading parameters and plate dimensions remained the same as in Section 3.2.

The strain distributions under various loading parameters exhibited very similar trends. The results under one set of loading parameters are analyzed in detail here as an example. Figure 11 shows the inherent strain distribution along Path 2 obtained after performing TEP-FE analysis and linear superposition of a single-line loading path. At $W = 50$ mm, the longitudinal out-of-plane, transverse in-plane, and transverse out-of-plane strain for the TEP-FE analysis and the linear superposition of the single loading path were essentially the same. Still, the longitudinal in-plane strain for the TEP-FE analysis was about half of that of the linear superposition of the single-line loading. At $W = 150$ mm, each strain component of the parallel loading line was consistent with the single-line loading linear superposition. The strain distribution of Path 1 was similar to that of Path 2. At $W = 50$ mm, which coincided with the case where the spacing of the loading lines was

smaller than the diameter of the induction heating source, the plastic zones of the front and rear loading lines overlapped. This shows that the effect of parallel loading lines on the strain distribution mainly occurred when the spacing of the two loading lines was less than the diameter of the induction heating source. When the spacing of the loading lines exceeded the diameter of the induction heating element, the plastic zones of the two loading lines before and after did not overlap, or the overlap area was relatively small, and the strain distribution was consistent with the linear superposition of the single-line loading.

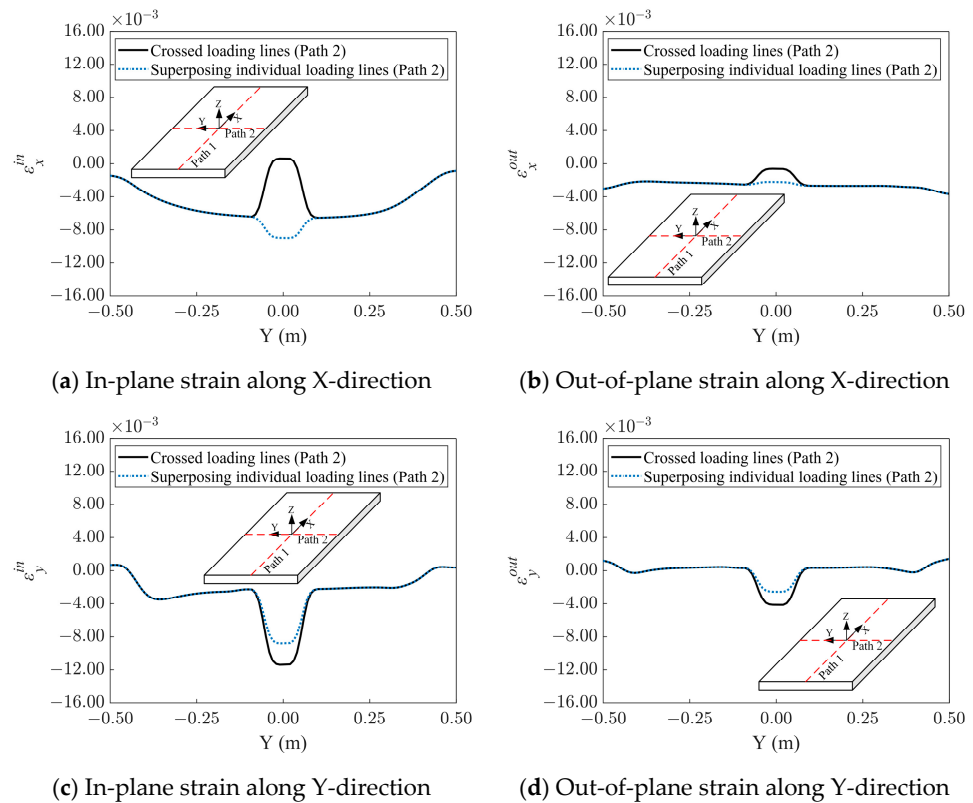


Figure 9. Comparison between results of plastic strain obtained from TEP-FE analysis of crossed loading lines and by superposing individual loading lines.

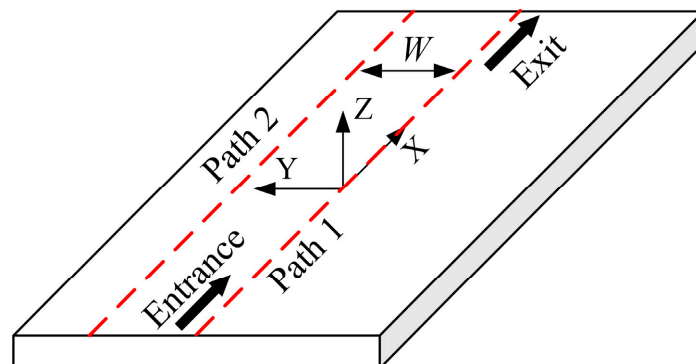


Figure 10. Schematic diagram of parallel loading line.

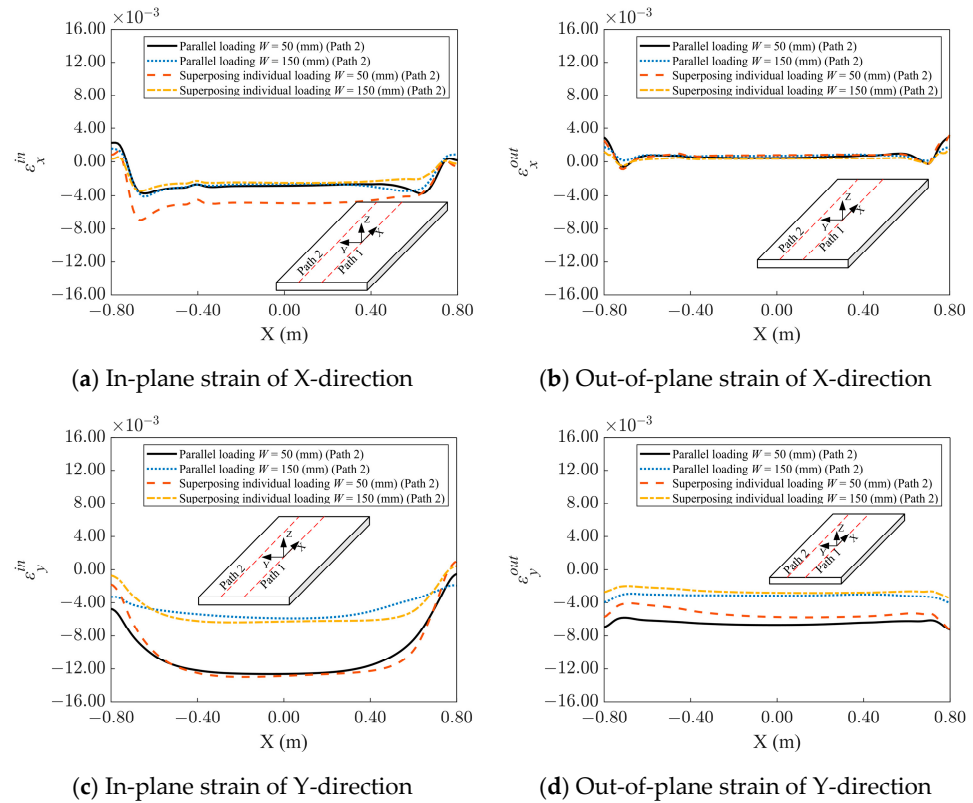


Figure 11. Comparison between results of plastic strain obtained from TEP-FE analysis and by superposing individual loading lines.

4. Multipath Process-Based Inherent Strain Method

4.1. Original Concept of the ISM

Based on TPE-FE analyses and experimental observations, researchers have pointed out that a source resulting in deformation must exist in the loading path and its immediate region [14]. This source is known as inherent strain. Inherent strain is a generic name for inelastic strains, such as plastic, thermal, and creep strains. Typically, thermal strains will disappear when the plate is cooled to room temperature. For mild steel used in shipbuilding, creep strain is negligible [14]. Therefore, the inherent strain of the plate in the IHMRF process is equivalent to the plastic strain. The inherent strain reflects the complex stress–strain evolution in the material during processing. Therefore, when applying the inherent strain to an elastic body, some complex features, such as temperature dependence of material properties and thermo-mechanical–plastic flow, are naturally considered.

Let ϵ^* denote inherent strain, and then the ϵ_e is equal to total strain ϵ minus the inherent strain,

$$\epsilon_e = \epsilon - \epsilon^* \tag{1}$$

The constitutive equation is written as

$$\sigma = C_0 : \epsilon_e = C_0 : (\epsilon - \epsilon^*) \tag{2}$$

where C_0 is a constant stiffness tensor at room temperature. Then, from the equilibrium equation

$$\nabla \cdot \sigma = 0 \tag{3}$$

it can be derived that

$$\nabla \cdot \tilde{\sigma} = f \tag{4}$$

where $\tilde{\sigma} = \nabla \cdot (C_0 : \epsilon)$ is the equilibrium stress and $f = \nabla \cdot (C_0 : \epsilon^*)$ is the resultant body force contributed by the inherent strain.

The above deduction shows that the application of the inherent strain can convert a thermo-elastic-plastic problem into a purely elastic problem. Therefore, the deformation may be computed using an elastic constitution if the inherent strain is known. In the deformation field analysis, the plate is considered an elastomer obeying Hooke’s law, and the deformation is obtained by static equilibrium analysis. The intrinsic strain is applied to the plate as an initial strain. However, the original ISM ignores the strain change at the loading path’s beginning and end. In addition, the effect of the multipath loading process is not considered, and the inherent strain is simply linearly superimposed. As mentioned earlier, although the existing ISM has succeeded in efficiently predicting welding deformation, there is still much room for improvement, especially in predicting plate deformation for the IHMRF process.

4.2. Description of the MPISM

(1) Acquisition of inherent strain

The inherent strains can be obtained either experimentally or by the TEP-FEM. The TEP-FEM (presented in Section 3.1) was used in the examples covered in this paper. According to Section 3.3, a slight change in the inherent strain occurs only in a very narrow range relative to the overall area of the plate. The area of hull plates is usually huge, so the effect of changes in material constraints around the machining paths is negligible. For the loading paths at different locations, the inherent strain is obtained by loading at the center of the plate.

(2) Loading of inherent strain

Here, a model containing a loading path is used to illustrate how inherent strains can be applied to an elastic finite-element model. Typically, the inherent strain exists mainly in a relatively narrow region near the loading path. Depending on factors such as process parameters, material properties, and plate thickness, the width of the inherent strain distribution region may be slightly larger or smaller than the distribution scale of the heat source. However, the difference between the two is generally slight. In addition, although the inherent strain values vary in the transverse direction in a complex manner, the larger values are generally concentrated in the distribution scale of the heat source. For this reason, the concept of equivalent inherent strain distribution is proposed in this study. As shown in Figure 12, the equivalent inherent strain is applied in a region of width b near the loading path, and its value is constant along the transverse section. However, the equivalent inherent strain is different for each layer in the thickness direction of the plate. b is taken as the distribution scale of the heat source. For example, when the heat source is induction heating, b is taken as the diameter of the coil. Figure 12 shows the assumed distribution of equivalent inherent strains along the transverse and longitudinal directions. The distribution of strain in the plane is reduced to the form of a segmented linear transformation. The distribution of out-of-plane strains is reduced to a constant form.

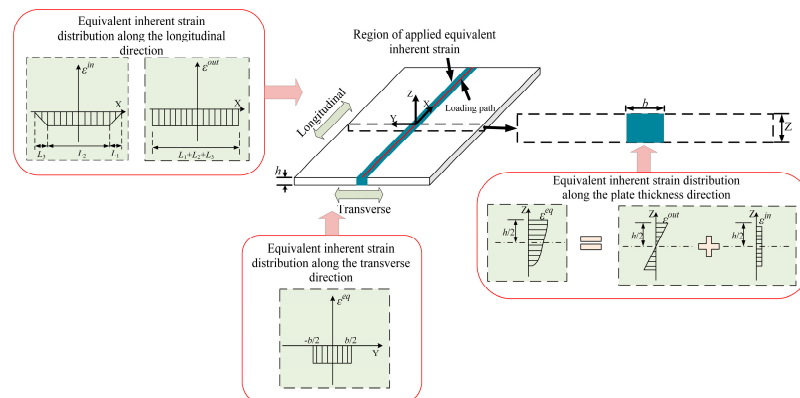


Figure 12. Schematic diagram of the region of applied equivalent inherent strain distribution.

The inherent forces and moments are obtained by integrating the inherent strains over the cross-section perpendicular to the loading path,

$$\begin{aligned}
 F_L &= \iint \frac{E}{1-\mu^2} (\varepsilon_L^* + \mu\varepsilon_T^*) dydz & F_T &= \iint \frac{E}{1-\mu^2} (\varepsilon_T^* + \mu\varepsilon_L^*) dydz \\
 M_L &= \iint \frac{Ez}{1-\mu^2} (\varepsilon_L^* + \mu\varepsilon_T^*) dydz & M_T &= \iint \frac{Ez}{1-\mu^2} (\varepsilon_T^* + \mu\varepsilon_L^*) dydz
 \end{aligned}
 \tag{5}$$

where F_L and F_T are the longitudinal and transverse inherent forces, respectively. M_L and M_T are the longitudinal and transverse inherent moments, respectively. E is Young’s modulus and μ is Poisson’s ratio. ε_L^* and ε_T^* are the longitudinal and transverse inherent strains, respectively. According to the plate-and-shell theory, the strains can be divided into out-of-plane strains that vary linearly along the thickness direction and in-plane strains that are constant along the thickness [15],

$$\varepsilon_L^{eq} = \varepsilon_L^{in} + \frac{2z}{h} \varepsilon_L^{out} \quad \varepsilon_T^{eq} = \varepsilon_T^{in} + \frac{2z}{h} \varepsilon_T^{out}
 \tag{6}$$

where ε_L^{in} and ε_L^{out} are the longitudinal equivalent in-plane and out-of-plane strains, and ε_T^{in} and ε_T^{out} are the transverse equivalent in-plane and out-of-plane strains, respectively. According to the principle of equivalence of inherent force and inherent moment,

$$\begin{aligned}
 F_L &= \iint \frac{E}{1-\mu^2} (\varepsilon_L^{eq} + \mu\varepsilon_T^{eq}) dydz = C_1 (\varepsilon_L^{in} + \mu\varepsilon_T^{in}) \\
 F_T &= \iint \frac{E}{1-\mu^2} (\varepsilon_T^{eq} + \mu\varepsilon_L^{eq}) dydz = C_1 (\varepsilon_T^{in} + \mu\varepsilon_L^{in}) \\
 M_L &= \iint \frac{Ez}{1-\mu^2} (\varepsilon_L^{eq} + \mu\varepsilon_T^{eq}) dydz = C_2 (\varepsilon_L^{out} + \mu\varepsilon_T^{out}) \\
 M_T &= \iint \frac{Ez}{1-\mu^2} (\varepsilon_T^{eq} + \mu\varepsilon_L^{eq}) dydz = C_2 (\varepsilon_T^{out} + \mu\varepsilon_L^{out})
 \end{aligned}
 \tag{7}$$

where $C_1 = (bEh)/(1 - \mu^2)$ and $C_2 = (bEh^2)/(6(1 - \mu^2))$. Substituting Equation (6) into Equation (7) deduces that,

$$\varepsilon_L^{eq} = \frac{F_L - \mu F_T}{C_1(1-\mu^2)} + \frac{2z(M_L - \mu M_T)}{C_2h(1-\mu^2)} \quad \varepsilon_T^{eq} = \frac{F_T - \mu F_L}{C_1(1-\mu^2)} + \frac{2z(M_T - \mu M_L)}{C_2h(1-\mu^2)}
 \tag{8}$$

Therefore, the value of the equivalent inherent strain can be obtained by Equations (5) and (8).

(3) Strain correction strategy

According to Section 3.4, crossing or proximity between loading paths can affect the inherent strain in the case of multiple loading paths. However, considering these effects are relatively concentrated, they can be corrected appropriately. For the IHMRP process covered in this paper, the following treatment is applied to the elasticity calculations for multiple loading paths:

- For the case where the previous and subsequent loading paths do not intersect and are widely spaced (spaced beyond the geometry of the heat source), the value calculated according to Equation (8) is applied in the vicinity of the loading paths with a width of b .
- For the case where the previous and subsequent loading paths cross or are spaced beyond the distribution range of the induced heat source, the variation of the inherent strain is neglected and the equivalent inherent strain calculated according to Equation (8) is applied to each loading path.
- For the case where the previous and subsequent loading paths cross, a square cross-impact zone centered on the crossing point with a width of b is defined. Within the cross-impact zone, the following strains are applied:

$$\begin{aligned}
 \epsilon_{pre}^{in} &= 0 \\
 \epsilon_{sub}^{in} &= \epsilon_{Tpre}^{in} + \epsilon_{Lsub}^{in} \\
 \epsilon_{pre}^{out} &= 0.5 \left(\epsilon_{Lpre}^{out} + \epsilon_{Tsub}^{out} \right) \\
 \epsilon_{sub}^{out} &= \epsilon_{Tpre}^{out} + \epsilon_{Lsub}^{out}
 \end{aligned}
 \tag{9}$$

where ϵ_{pre}^{in} and ϵ_{pre}^{out} are the in-plane and out-of-plane strains in the cross-impact zone along the direction of the previous loading path, ϵ_{sub}^{in} and ϵ_{sub}^{out} are the in-plane and out-of-plane strains in the cross-impact zone along the direction of the subsequent loading path, ϵ_{Tpre}^{in} and ϵ_{Tpre}^{out} are the transverse in-plane and out-of-plane strains of the previous loading path calculated according to Equation (8), ϵ_{Lpre}^{in} and ϵ_{Lpre}^{out} are the longitudinal in-plane and out-of-plane strains of the previous loading path calculated according to Equation (8), ϵ_{Tsub}^{in} and ϵ_{Tsub}^{out} are the transverse in-plane and out-of-plane strains of the subsequent loading path calculated according to Equation (8), and ϵ_{Lsub}^{in} and ϵ_{Lsub}^{out} are the longitudinal in-plane and out-of-plane strains of the subsequent loading path calculated according to Equation (8).

- For the case where the spacing between the previous and subsequent loading paths is less than the diameter of the heating source, the longitudinal out-of-plane strain and the transverse in-plane and out-of-plane strains for each loading path are imposed as calculated in accordance with Equation (8), but the longitudinal in-plane strain for each load line is taken to be one half of that calculated in accordance with Equation (8).

(4) Elasticity analysis procedure

In the MPISM, the deformation field of the plate is obtained by elastic finite element analysis. In this study, the analysis procedure was developed based on commercial finite element software ABAQUS. The plate as a deformed body was simulated as a four-node shell element (named S4R in ABAQUS). The element size was 10 mm × 10 mm. Spring constraints were placed at the edges of the plate to avoid rigid displacement of the plate. Geometrical nonlinearities are considered in the analysis procedure and the loads were applied to the plate stepwise in incremental application. The size of the incremental step was determined using the automatic incremental step algorithm provided in ABAQUS.

5. Results and Discussion

In this section, the accuracy and efficiency of the MPISM are verified by predicting the deformation in two hull plates fabricated by IHMRF. In the first example, multiple loading paths with different directions are set to cross at different plate positions. The results of experimental measurements and the MPISM were compared. The second example involved setting up several loading paths in the same direction at various distances from the plate edge, with the spacing between the multiple loading paths gradually changing. Comparing results with the TEP-FEM further confirmed the accuracy and efficiency of the MPISM.

5.1. Comparison with Experimental Results

In the first example, the dimensions of the mild steel plate were 2000 mm × 1000 mm × 16 mm. A schematic diagram of the loading paths arrangement is shown in Figure 13. The loading sequence was executed in descending order of numbering. The loading tool parameters for each loading path are shown in Table 2. Figure 14 shows a photograph of the experimental procedure.

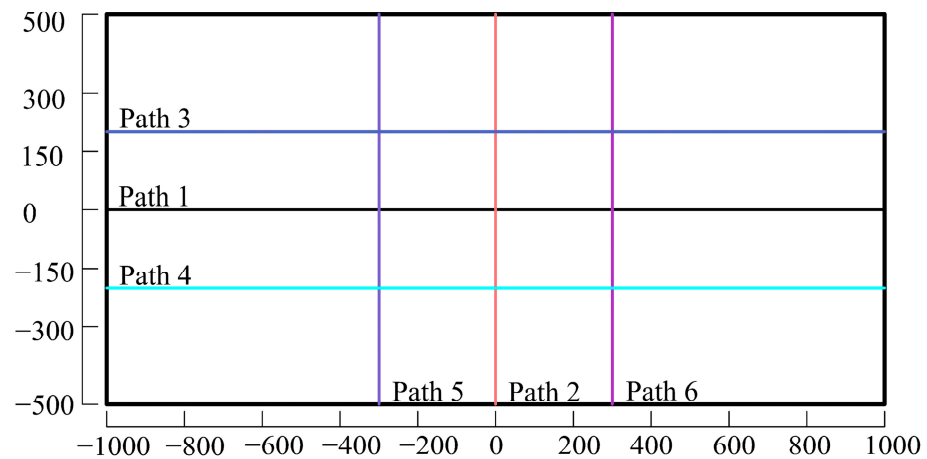


Figure 13. Schematic diagram of the loading lines.

Table 2. Loading parameters for the saddle-type plate.

Path Number	Starting Coordinates	End Coordinates	Power (kW)	Forming Depth (mm)	Velocity (mm/s)
1	(−950, 0)	(950, 0)	20.0	3.0	2.0
2	(−950, −200)	(950, −200)	20.0	2.0	4.0
3	(−950, 200)	(950, 200)	20.0	2.0	4.0
4	(0, −400)	(0, 400)	24.0	3.0	2.0
5	(−300, −400)	(−300, 400)	18.0	2.0	2.0
6	(300, −400)	(300, 400)	18.0	2.0	2.0

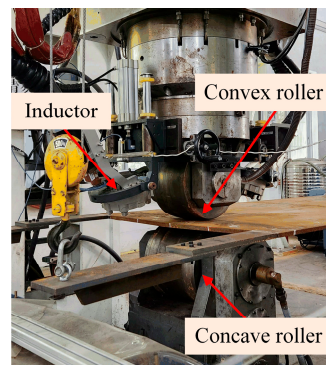


Figure 14. Photograph of the experimental procedure.

The primary method used in the hull plate forming process to assess if the plate satisfies design specifications is to compare the deflection of the plate. Figure 15 displays the plate deflections in both transverse and longitudinal directions. Regarding the direction and size of the deflections, the MPISM predictions and experimental results coincide. Table 3 summarizes the relative errors for the maximal deflections. The highest relative error between the MPISM and the experiment is 16.4% for the maximal deflection in the longitudinal direction. The highest relative error between the MPISM and the experiment for the maximum transverse deflection is 8.9%. The longitudinal deflection has a significant amount of inaccuracy. The accuracy of the obtained inherent strain may affect this. It is typically assumed that the material is isotropic and that its properties are uniform throughout the plate in the TEP-FE model for obtaining inherent strains. However, the actual material properties of the plates may be anisotropic and inhomogeneous. Since it is difficult to fully account for the actual material properties in the TEP-FEM, the accuracy

of the obtained inherent strains may be decreased. However, overall, the accuracy of the MPISM meets the requirements of engineering practice.

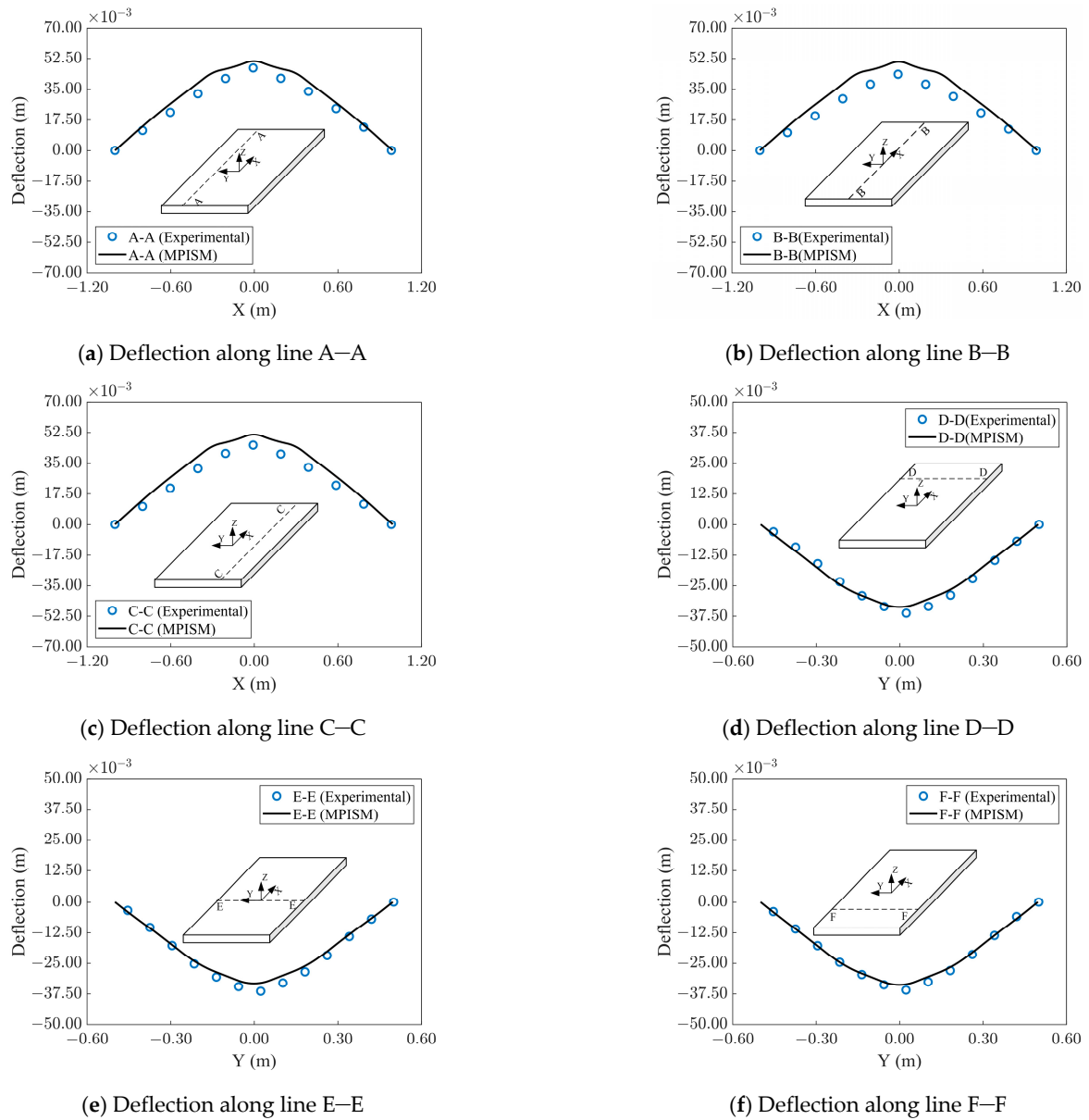


Figure 15. Comparison of the deflection of the plate between experiment measurements and the MPISM.

Table 3. The relative error between the predictions of the MPISM and experimental results.

A–A	B–B	C–C	D–D	E–E	F–F
8.2%	16.4%	13.2%	6.5%	8.9%	6.1%

5.2. Comparison of the TEP-FEM and ISM

In the second example, the plate was 2000 mm × 1000 mm × 16 mm. Figure 16 illustrates the loading path arrangement. The loading parameters were as follows: 2 mm forming depth of the rollers, 20 kW power of the induction heat source, and 2 mm/s movement speed of the plate.

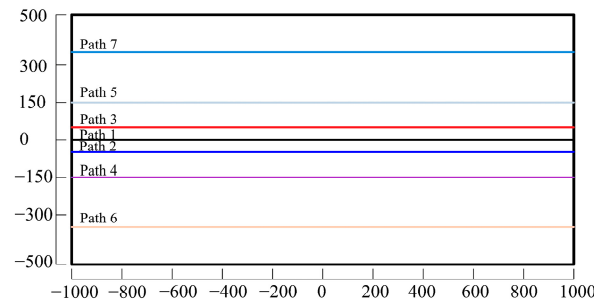


Figure 16. Schematic diagram of the parallel loading lines.

The vertical deformation displacements of the plates, as predicted by the MPISM and TEP-FEM, are displayed in Figure 17. The consistency of the predicted results obtained from both strategies is evident. Figure 18 compares the deflection to investigate the accuracy of the MPISM further. Both the deflection trend and the deflection magnitude are consistent between the results of the MPISM and TEP-FEM, as can be seen. The highest relative error between the MPISM and TEP-FEM for the longitudinal deflection is 6.9%. The highest relative error between the MPISM and TEP-FEM for transverse deflection is 4.1%. On the other hand, the TEP-FEM and the original ISM diverge significantly. Paths 1–3 in Figure 16 are in close proximity to each other, and the longitudinal in-plane strains are affected (see Section 3.4 for related analyses). However, no strain correction is considered in the original ISM. Therefore, while the original ISM predicts transverse deformation with good accuracy, it predicts longitudinal deformation with poor accuracy. The MPISM considers the impact of the multipath sequential loading process on the inherent strain, which is a critical distinction between it and the original ISM.

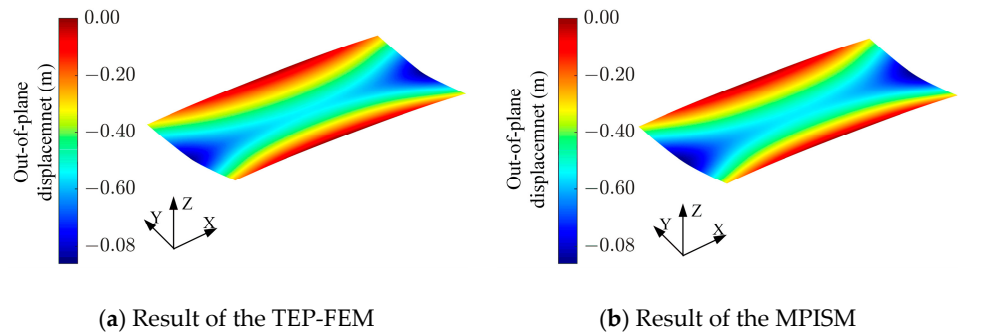


Figure 17. Contour plots of vertical deformation displacement predicted by the TEP-FEM and MPISM.

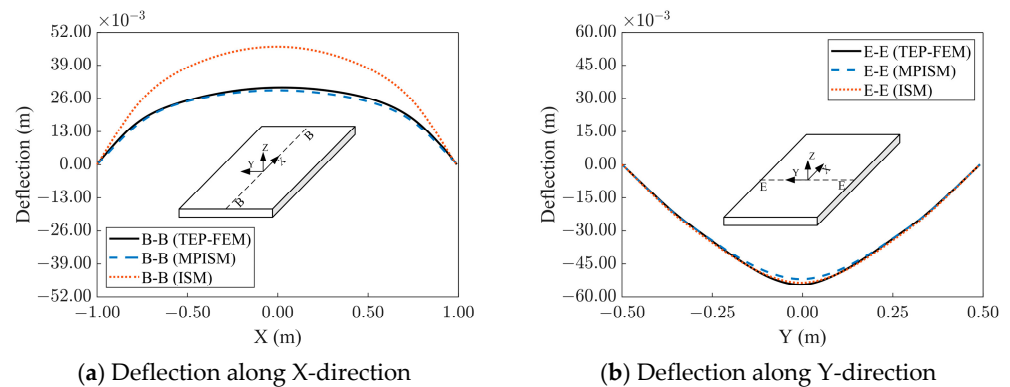


Figure 18. Comparison of the predictions between the TEP-FEM, MPISM, and ISM.

The time spent by the TEP-FEM, MPISM, and ISM is displayed in Table 4. The MPISM outperformed the TEP-FEM in terms of efficiency when both use the same computational

resource. The time used by the MPISM was slightly greater than that of the original ISM. However, the accuracy of the MPISM surpasses the original ISM by a large margin.

Table 4. Computational times for the TEP FEM, MPISM, and ISM.

Element Number	Node Number	Method	Time (min)
20,000	20,301	TEP-FEM	376
		MPISM	0.3
		ISM	0.2

6. Conclusions

In this paper, a multipath process-based inherent-strain method (MPISM) is proposed for efficient prediction of plate deformation by the IHMRF process. The accuracy and effectiveness of the MPISM were verified by experimental results and results of the TEP-FEM. The main conclusions are as follows:

- (1) The inherent strain in the plate during IHMRF is characterized by the following: in the longitudinal direction, the inherent strain varies only near the beginning and end of the processing path and tends to be constant in the middle region; in the transverse direction, the larger values of the inherent strain are concentrated in the range of the heat source geometry.
- (2) The position of the loading path relative to the edge of the plate has a negligible effect on the inherent strain of the plate during IHMRF.
- (3) For loading path crossings, the main effect on strain occurs near the intersection point, whereas loading paths close to each other affect the longitudinal out-of-plane strain across the loading path.
- (4) The MPSIM significantly improves efficiency while maintaining accuracy consistent with the TEP-FEM. Compared with the original ISM, the MPISM improves accuracy while maintaining efficiency by taking into account the distributional characteristics of the actual inherent strains as well as the effects of the multipath sequential loading process.

Author Contributions: Z.W.: conceptualization, methodology, software, validation, and writing—original draft; Y.Z.: conceptualization, methodology, and writing—review and editing; H.Y.: investigation and writing—review and editing; L.C.: validation, investigation, and writing—review and editing. All authors have read and agreed to the published version of the manuscript.

Funding: This research received no external funding.

Institutional Review Board Statement: Not applicable.

Informed Consent Statement: Not applicable.

Data Availability Statement: Data are contained within the article.

Conflicts of Interest: The authors declare no conflicts of interest.

References

1. Shin, J.G.; Ryu, C.H. Nonlinear Kinematic Analysis of the Deformation of Plates for the Ship Hull Fabrication. *J. Ship Res.* **2000**, *44*, 270–277. [[CrossRef](#)]
2. Lee, K.S.; Hwang, B. An approach to triangular induction heating in final precision forming of thick steel plates. *J. Mater. Process. Technol.* **2014**, *214*, 1008–1017. [[CrossRef](#)]
3. Zhao, Y.; Yuan, H.; Tang, G.; Dong, H.; Hu, C.; Yan, J. Automatic Integral Forming Method for Double-Curvature Plate of Ship. U.S. Patent 9751123 B2, 5 September 2017.
4. Liang, W.; Hu, X.; Zheng, Y.; Deng, D. Determining inherent deformations of HSLA steel T-joint under structural constraint by means of thermal elastic plastic FEM. *Thin-Walled Struct.* **2019**, *147*, 106568. [[CrossRef](#)]
5. Wei, Z.; Zhao, Y.; Yuan, H.; Chang, L. Equivalent load model for the numerical simulation of integrated induction heating and mechanical rolling forming of curved hull plates. *Int. J. Adv. Manuf. Technol.* **2024**, *130*, 3891–3903. [[CrossRef](#)]

6. Wang, C.; Pham, D.T.; Wu, C.; Kim, J.-W.; Su, S.; Jin, Z. Artificial thermal strain method: A novel approach for the analysis and fast prediction of the thermal distortion. *J. Mater. Process. Technol.* **2021**, *289*, 116937. [[CrossRef](#)]
7. Liang, W.; Murakawa, H. An inverse analysis method to estimate inherent deformation in thin plate weld joints. *Mater. Des.* **2012**, *40*, 190–198. [[CrossRef](#)]
8. Huang, H.; Wang, J.; Li, L.; Ma, M. Prediction of laser welding induced deformation in thin sheets by efficient numerical modeling. *J. Mater. Process. Technol.* **2016**, *227*, 117–128. [[CrossRef](#)]
9. Yi, B.; Zhou, X.; Shen, C.; Wang, J. Computational investigation on transient thermal tensioning for mitigation of welding induced buckling by elastic FE method. *J. Manuf. Process.* **2022**, *83*, 590–606. [[CrossRef](#)]
10. Wang, J.; Yi, B.; Zhang, C.; Zhou, H.; Shu, Y. Experiments of double curvature plate bending with induction heating and processing parameters investigation by computational analysis. *Ocean Eng.* **2019**, *192*, 106596. [[CrossRef](#)]
11. Zhao, Y.; Hu, C.; Dong, H.; Yuan, H. Automated local line rolling forming and simplified deformation simulation method for complex curvature plate of ships. *Mech. Sci.* **2017**, *8*, 137–154. [[CrossRef](#)]
12. Liang, X.; Chen, Q.; Cheng, L.; Hayduke, D.; To, A.C. Modified inherent strain method for efficient prediction of residual deformation in direct metal laser sintered components. *Comput. Mech.* **2019**, *64*, 1719–1733. [[CrossRef](#)]
13. Vega, A.; Rashed, S.; Murakawa, H. Analysis of cross effect on inherent deformation during the line heating process—Part 1—Single crossed heating lines. *Mar. Struct.* **2015**, *40*, 92–103. [[CrossRef](#)]
14. Deng, D.; Murakawa, H.; Liang, W. Prediction of welding distortion in a curved plate structure by means of elastic finite element method. *J. Mater. Process. Technol.* **2008**, *203*, 252–266. [[CrossRef](#)]
15. Timoshenko, S.; Woinowsky-krieger, S. *Theory of Plates and Shells*; McGraw-Hill Book Company: New York, NY, USA, 1959; pp. 378–383.

Disclaimer/Publisher’s Note: The statements, opinions and data contained in all publications are solely those of the individual author(s) and contributor(s) and not of MDPI and/or the editor(s). MDPI and/or the editor(s) disclaim responsibility for any injury to people or property resulting from any ideas, methods, instructions or products referred to in the content.